Results in Physics 48 (2023) 106403

Contents lists available at ScienceDirect

Results in Physics

journal homepage: www.elsevier.com/locate/rinp

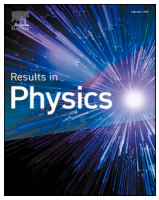

Synthesis and optical properties of polyvinylidene difluoride nanocomposites comprising MoO3/g-C3N4

Sultan Alhassan [a], Khulaif Alshammari [a], Majed Alshammari [a], Turki Alotaibi [a], Alhulw H. Alshammari [a], Yasir Fawaz [a], T.A. Taha [a], Mohamed Henini [b]

[a] Physics Department, College of Science, Jouf University, P.O. Box:2014, Sakaka, Saudi Arabia
[b] School of Physics and Astronomy, University of Nottingham, Nottingham NG7 2RD, UK

ARTICLE INFO

Keywords:
Polyvinylidene difluoride
MoO_3/g-C_3N_4
Optical band gap
Refractive index

ABSTRACT

The present study describes the optical properties for prepared polymer nanocomposites of PVDF at different content of MoO_3/g-C_3N_4. The structural properties of polymer films were analysed via XRD, FTIR and ESEM techniques. The XRD diffraction patterns of PVDF with different concentrations of MoO_3/g-C_3N_4 have two characteristic peaks at 2 θ = 18.4° and 20.3° where first peak was assigned to α-phase, while last peak was attributed to β-phase. The ESEM micrographs of PVDF-MoO_3/g-C_3N_4 nanocomposites have shown smooth surface topography. According to the UV–visible absorption spectra, the UV absorption of PVDF was increased when adding MoO_3/g-C_3N_4 nanoparticles where distinct peak was appeared in the UV region at 310 nm and its edges become more intense and moved towards higher wavelength after MoO_3/g-C_3N_4 incorporation. The optical values of (E_{dir}) and (E_{ind}) energies have decreased with increasing the nanoparticle composites content. The optical band gap energy (E_{opt}) was decreasing from 5.66 eV to 4.56 eV as increasing the content of MoO_3/g-C_3N_4. The refractive index (n) was increased with increasing the concentration of MoO_3/g-C_3N_4 in nanocomposites samples, except for the sample with 0.25 wt%. The distinctive optical characteristics of PVDF-MoO_3/g-C_3N_4 qualify such polymer nanocomposites for optoelectronic applications.

Introduction

The different applications of polymer nanocomposites require materials with distinct properties. Therefore, researchers seek to develop polymer compounds by treating them with nanomaterials of different sizes, shapes, and content [1–4]. The importance of nanomaterials integration into polymer matrices lies in achieving distinctive properties at low concentrations. Nanomaterials are found in different shapes such as nanosheet, nanotube, nanoparticles and nanorod. The polymer/nanomaterial interface determine the optical and dielectric properties. The polymerization of vinylidene difluoride monomer produce polyvinylidene difluoride (PVDF) polymer. PVDF polymer has the chemical formula –CH_2–CF_2– and includes α, β, γ, δ and ε crystalline phases [5–7]. This structure induces ferroelectricity, piezoelectricity, pyroelectricity, and optical properties of PVDF polymer [8]. From an application standpoint, the polar β phase of PVDF is the most suited polymer phase for improving ferroelectric, piezoelectric, and pyroelectric characteristics. Actually, the polymorphic β phase and other phases always coexist at crystallization of PVDF. The factors that control the growth of β phase are the temperature, type of polar solvent, mechanical stretching, nanomaterials type and DC electric poling [9,10]. Among the nanomaterials, ferrite enhance the crystallization of β phase at low filler content. Therefore, PVDF polymer composites containing nanoferrites produce ferroelectricity and strong magnetoelectric properties [11].

High optical performance polymers are required for many applications. Thus, flexible PVDF polymer nanocomposites films with improved optical properties were investigated in the literature. Ajay Pal Indolia and M. S. Gaur [12] have studied the optical spectroscopy parameters of PVDF-ZnO polymer films. At concentrations of ZnO (0.0–9.0 wt%) the direct optical energy gap decreased from 5.66 to 4.95 eV. Moreover, the values of indirect energy gap decreased from 4.96 to 3.35 eV. However, the refractive index of these polymer films increased from 1.51 to 1.71. Maheswar Panda et al. [13] have prepared different samples of PVDF-GO nanocomposite films. Moreover, the optical absorption of these polymer films improved with the addition of GO. The refractive index of PVDF-GO nanocomposite films revealed variations with the content of GO. PVDF-$Li_4Ti_5O_{12}$ nanocomposite films were prepared and subjected to optical absorption measurements [14]. The concentrations of

E-mail address: ssalhassan@ju.edu.sa (S. Alhassan).

https://doi.org/10.1016/j.rinp.2023.106403
Received 12 February 2023; Received in revised form 24 March 2023; Accepted 27 March 2023
Available online 30 March 2023

$Li_4Ti_5O_{12}$ increased from 0.0 to 2.0 wt%. Accordingly, the direct optical energy gaps decreased from 5.567 to 4.858 eV and in case of indirect energy gaps (3.625 to 1.005 eV). Further, the refractive index and optical susceptibility for these nanocomposite films were highly improved as the percent of $Li_4Ti_5O_{12}$ increased. Mai M. El-Masry and Rania Ramadan [15] have studied the optical properties of PVDF polymer nanocomposites at different filler ratios of $CoFe_2O_4$, $CuFe_2O_4$ and Cu/$CoFe_2O_4$ nanomaterials. The data analysis of optical spectroscopy showed a reduction of optical energy gaps when the content of nanoparticles increase. Moreover, the addition of $CoFe_2O_4$, $CuFe_2O_4$ and Cu/$CoFe_2O_4$ enhanced the optical conductivity of PVDF polymer films. PVDF/Mg polymer nanocomposites were investigated at different filler content (0.0–8.0 wt%) of $MgCl_2$ [16]. The optical absorption data for these films showed a gradual decrease with increasing filler content. The optical energy gaps increased from 0.36 to 1.99 eV as the concentration of $MgCl_2$ increased.

The nanoparticles of molybdenum oxide (MoO_3) are inexpensive, environmentally friendly and showed high optical activity [17,18]. Further, MoO_3 showed high performance of photovoltaics, light emitting diodes (OLEDs) and field effect transistor (FET) [19]. Combining MoO_3 with g-C_3N_4 is expected to show high optical performance of composites. This comes because g-C_3N_4 nanosheet has a small energy gap (2.7 eV) and show improved optical, electronic and catalytic performance [20–22].

The present study aims at preparing polymer nanocomposites of PVDF at different content of MoO_3/g-C_3N_4. The structural properties of polymer films was analysed according to XRD, FTIR and ESEM measurements. Moreover, the optical absorption spectroscopy data of the PVDF-MoO_3/g-C_3N_4 were completed concerning linear and nonlinear optical parameters. The performance of nanofiller at energy gap, refractive index and optical susceptibly was investigated at different content (0.0–1.0 wt%).

Experimental

The thermal polycondensation technique was applied to prepare g-C_3N_4 nanosheets. 10 g of Urea were treated thermally at 500 °C for 2 h at a heating rate of 2.0 °C/min. On the other hand, MoO_3/g-C_3N_4 nanocomposite was prepared via ultrasonic treatment of 90% MoO_3 and 10 % g-C_3N_4 in ethanol for 2 h. The PVDF/MoO_3/g-C_3N_4 blend films prepared by solution casting method. The PVDF powder was dissolved in 1:1 DMF/acetone mixture for 2 h at 50 °C. After this step, the powder of MoO_3/g-C_3N_4 was dispersed in 5.0 mL acetone and then integrated to PVDF clear solution. Moreover, the mixture was stirred for 1.0 h at 50.0 °C. Finally, the solutions of PVDF/MoO_3/g-C_3N_4 were transferred to glass plates and dried at 100 °C overnight.

The crystal structure spectra of PVDF/MoO_3/g-C_3N_4 films were examined on XRD 7000 diffractometer, Shimadzu, Japan. The ATR spectra were collected from FTIR spectrometer–Tracer 100, Shimadzu, Japan. The ESEM micrographs were recorded on Quattro environmental scanning electron microscope (ESEM), Thermofisher, USA. The absorption spectra of blend films were extracted from Cary 60 UV–Vis spectrophotometer, Agilent, USA. A 270 nm excitation wavelength was used to produce photoluminescence (PL) spectra at room temperature using a Cary Eclipse fluorescence spectrometer.

Results and discussion

The XRD patterns peaks of polymer (PVDF) and nanocomposites (MoO_3/g-C_3N_4) are shown in Fig. 1(a). The XRD pattern at 2 θ = 12.8°, 23.4°, 25.6°, 27.4°, 33.8°, 39.2° and 49.4° of MoO_3/g-C_3N_4 correspond to (020), (110), (040), (021), (111), (060) and (002) planes, respectively. The characteristic peaks of MoO_3/g-C_3N_4 belong to data of the orthorhombic structure and agree with JCPDF card number (05-0508) [23]. Moreover, the average crystal size (D) produced from Scherer equation based on the full width at half maximum (β) for the

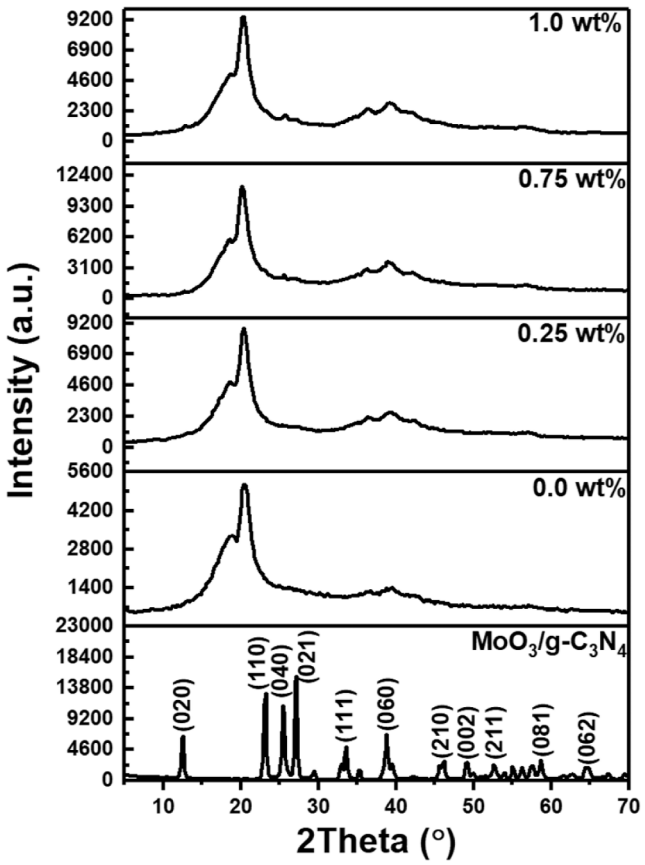

Fig. 1. XRD diffraction patterns of PVDF polymer nanocomposites modified with MoO_3/g-C_3N_4.

diffraction peaks recorded in Fig. 1 [24,25];

$$D = 0.9\lambda/\beta cos\theta \quad (1)$$

where λ = 1.54056 Å and θ is the diffraction angle. Accordingly, the average crystal size of MoO_3/g-C_3N_4 was 18 nm.

PVDF is a semicrystalline polymer with two basic crystal phases, namely α and β crystalline [26,27]. The diffraction patterns of PVDF with different content of MoO_3/g-C_3N_4 observed two characteristic peaks at 2 θ = 18.4° and 20.3°, which correspond to (020) and (110) crystal planes, respectively. The appearance of a shoulder peak at 18.4° assigned to α-phase, while the broad diffraction peak at 20.3° attributed to β-phase. Moreover, the intensity of the peak indexed to β-phase improved up to 0.75 wt% and then decreased at 1.0 wt% of MoO_3/g-C_3N_4. This improvement indicated the obstruction of PVDF crystallinity chain movement. The crystallinity index for these nanocomposite films could be estimated from the relation (X_c(%) = (Area under crystalline peaks/Area under all peaks) × 100). As a result, the crystallinity index was increased from 17 to 22% when the percentage of MoO_3/g-C_3N_4 raised from 0.0 to 1.0 wt%. This finding reveals the enhanced crystallinity of the PVDF/MoO_3/g-C_3N_4 films.

The FT-IR spectra of PVDF/MoO_3/g-C_3N_4 and different concentrations of MoO_3/g-C_3N_4 were recorded in the region 400–2000 cm^{-1} as shown in Fig. 1(b). The spectra bands appearing at 610, 770 and 950 cm^{-1} correspond to the PVDF α-phase, while bands at 510, 833, 1070, 1250 and 1405 cm^{-1} ascribed to the PVDF β-phase. The bands at 510, 610, and 770 cm^{-1} attributed to the bending vibration of CF_2, while the band at 833 cm^{-1} related to the rocking vibration of CH_2 [28]. In accordance with the CH and CF out-of-plane deformations, the bands arise at 950 and 1230 cm^{-1}, respectively. The peaks at around 1400 cm^{-1} correspond to the C–H deformation vibration, while the peak at around 1071 cm^{-1} attributed to the C–F vibration, respectively [29].

Moreover, the positions of the absorption bands slightly moved to higher wavenumber as the content of MoO_3/g-C_3N_4. This is evidence of the bonding between the PVDF polymer matrix and the nanofiler by hydrogen bonds (Fig. 2).

The ESEM micrographs of PVDF-MoO_3/g-C_3N_4 nanocomposites comprising 0.0, 0.25, 0.75 and 1.0 wt% were depicted in Fig. 3. The provided scans declare spherulite surface topography. Moreover, the dispersion of MoO_3/g-C_3N_4 is dominated in the images of Fig. 3. The surface roughness (R_q) values estimated via ImageJ software were 34.36, 38.19, 45.58 and 48.61 for the content of MoO_3/g-C_3N_4 0.0, 0.25, 0.75 and 1.0 wt%.

The optical properties have been measured by UV–Visible spectroscopy for the PVDF- MoO_3/g-C_3N_4 nanocomposites consisting of 0.0, 0.25, 0.75, and 1 wt% of MoO_3/g-C_3N_4. The UV–Visible absorption spectroscopy is a powerful method for examining the optical characteristics of materials. The UV–visible absorption spectra of pure PVDF (0 wt%) and PVDF/MoO_3/g-C_3N_4 nanocomposites at various MoO_3/g-C_3N_4 concentrations (wt%) are shown in Fig. 4. The curves of the high MoO_3/g-C_3N_4 concentration nanocomposites exhibit a distinct peak in the UV region and none absorption in the visible area. From Fig. 4(a), a sharp absorption edges become more intense and moved towards higher wavelength after MoO_3/g-C_3N_4 incorporation. Further, the optical absorption peak in nanocomposite samples is located approximately at 310 nm, which is a distinctive UV peak for MoO_3/g-C_3N_4. Further evidence that integrated MoO_3/g-C_3N_4 nanoparticles are relatively monodispersed confirmed from sharp absorption edges and well-developed excitonic peaks [30].

Fig. 4(b) shows the transmittance (T) vs wavelength spectra of PVDF-MoO_3/g-C_3N_4 nanocomposites within the ranges of 200–1000 nm. It can be seen from Fig. 4(b) that the transmittance decrease with increasing the concentration of MoO_3/g-C_3N_4. The observed decrease in transmittance is caused by an increase in surface roughness. The reduction in transmittance is explained by Rayleigh scattering occurred by MoO_3/g-C_3N_4, similar with case of ZnO nanocomposites or due to the oscillation of free surface electrons, metal particles exhibit high wavelength-dependent absorption in the visual range, even at small diameters [30]. Generally, the doping polymer with nanoparticles led to formation of absorption centres, which increased the absorbance while reducing the transmittance, as illustrated in Fig. 4(a and b).

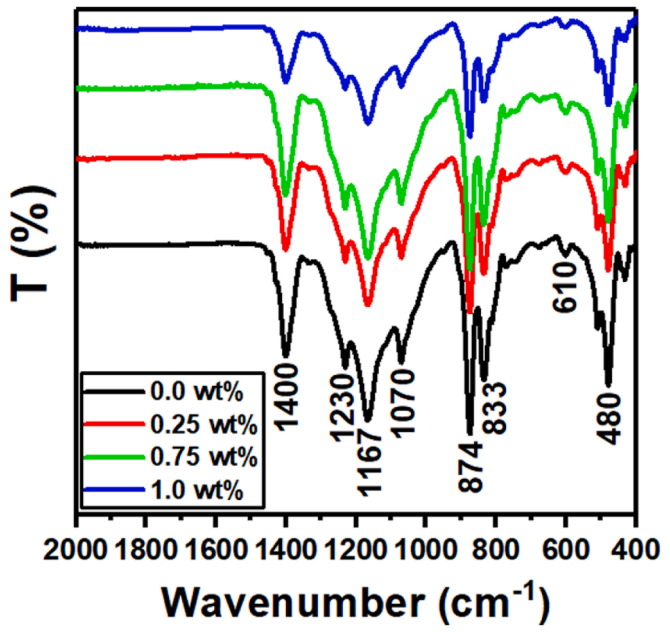

Fig. 2. FTIR spectra of PVDF polymer nanocomposites integrated with varying concentrations of MoO_3/g-C_3N_4.

Semicrystalline polymers have both direct and indirect band gaps because of electronic transitions near the band edge. The following equation uses the Tauc formula to obtain the optical band gap energy (E_{opt}) for allowed electronic transitions [31,32];

$$\alpha h\upsilon = k(h\upsilon - E_{opt})^x \quad (2)$$

where α is the absorption coefficient, $h\upsilon$ is the energy of photons and k represents the blend structure constant. The exponent x indicates direct and indirect allowed transitions with values of 0.5 and 2 respectively. The linear plot to the intercept is extrapolated to yield the values of band gap energies for both direct and indirect; as in Fig. 5(a and b). The experiment values of both direct (E_{dir}) and indirect (E_{ind}) energies are illustrated in Table 1. From Table 1, it can be seen that the optical values of (E_{dir}) and (E_{ind}) energies have decreased with increasing the nanoparticle composite content. The reduction of band gap energies in both direct (E_{dir}) and indirect (E_{ind}) could be related to the structural modifications which brought on by the addition of MoO_3/g-C_3N_4 may be responsible for this behaviour. As a result, a compositional dependence is found to affect the optical band gap (direct and indirect). Usually, the polymer nanocomposite thin film's electrical conductivity rises as a result of this modification, which denotes a narrowing of the energy band gap. Also, the drop in optical energy levels of nanocomposites are because of creation of deep defects and therefore affects the optical characteristics of materials [33,34].

It worth mentioning that, the optical band gap energy (E_{opt}) is decreasing as the content of MoO_3/g-C_3N_4 is increasing. This decrease in E_{opt} is assigned to the growth of structural disorder [14]. The existence of structural disorder, which increase the density of localized states, causing the Urbach tail to broaden and, as a result, reduce the energy gap.

The optical reflectance of pure PVDF and PVDF/MoO_3/g-C_3N_4 nanocomposites is shown in Fig. 6(a). The PVDF film has a lower reflectivity than PVDF-MoO_3/g-C_3N_4 nanocomposites. It worth to notice that, as MoO_3/g-C_3N_4 concentration in nanocomposites increased, the reflectance as well increased, indicating an improvement after addition of MoO_3/g-C_3N_4. In addition, at around 310 nm, the reflectance spectra are abruptly reduced, which is corresponded to the peak absorption of MoO_3/g-C_3N_4. Additionally, the optical reflectance spectra shown in Fig. 6(a) was utilized to calculate the refractive index (n) using Eq. [35];

$$n = \left(\frac{1+R}{1-R}\right) + \sqrt{\frac{4R}{(1-R)^2} - k^2} \quad (3)$$

where k is the extinction coefficient, and can be calculated using the formula $k = \alpha\lambda/4\pi$.

One of the most important variables in selecting the material for optical applications is the refractive index. The variation in refractive index (n) with wavelength for pure PVDF and PVDF/MoO_3/g-C_3N_4 nanocomposites is shown in Fig. 6(b). Pure PVDF film has a refractive index of around 3. As the concentration of MoO_3/g-C_3N_4 in nanocomposites samples increased, as the refractive index raised, except for the sample with 0.25 wt%, which observed decreasing in its refractive index. This may be explained because of reduced entanglement and fewer interactions between polymer chains and extra nanofiller minimize packing, resulting in a lower refractive index [36].

The refractive index of nanocomposites can be calculated by Eq. [37];

$$(n^2-1)^{-1} = \frac{E_0}{E_d} - \frac{1}{E_0 E_d}(h\upsilon)^2 \quad (4)$$

where hυ represents the photons energy, E_0, E_d and n are the single-oscillator energy, the dispersion energy, and the refractive index, respectively. Furthermore, the slope and intercept of the plot of $(n^2-1)^{-1}$ vs $(h\upsilon)^2$ can be used to determine the E_0 and E_d values, as illustrated in Fig. 7(a) and Table 2. Moreover, Fig. 7(b) show the relation

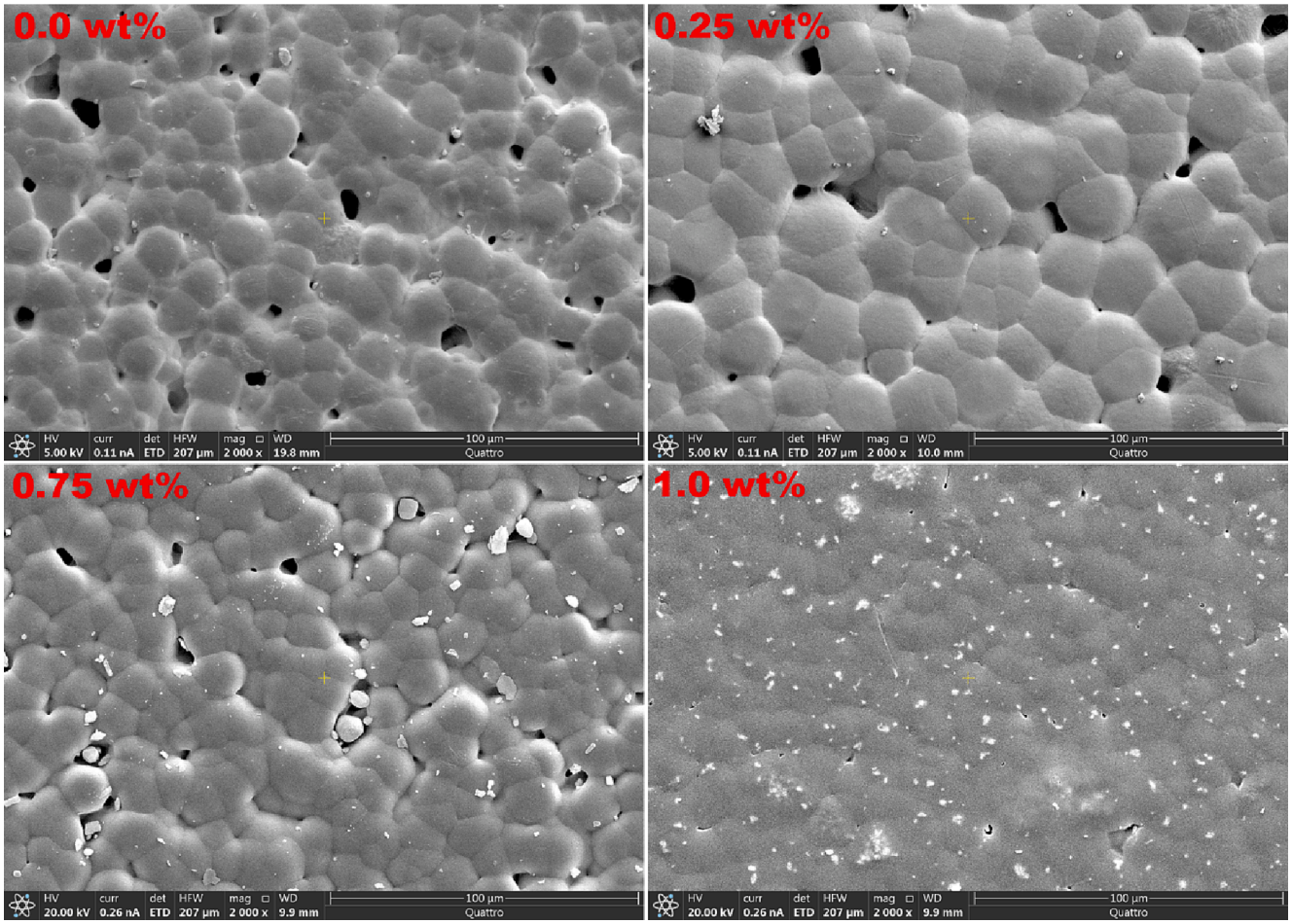

Fig. 3. The ESEM micrographs of PVDF polymer nanocomposites integrated MoO_3/g-C_3N_4.

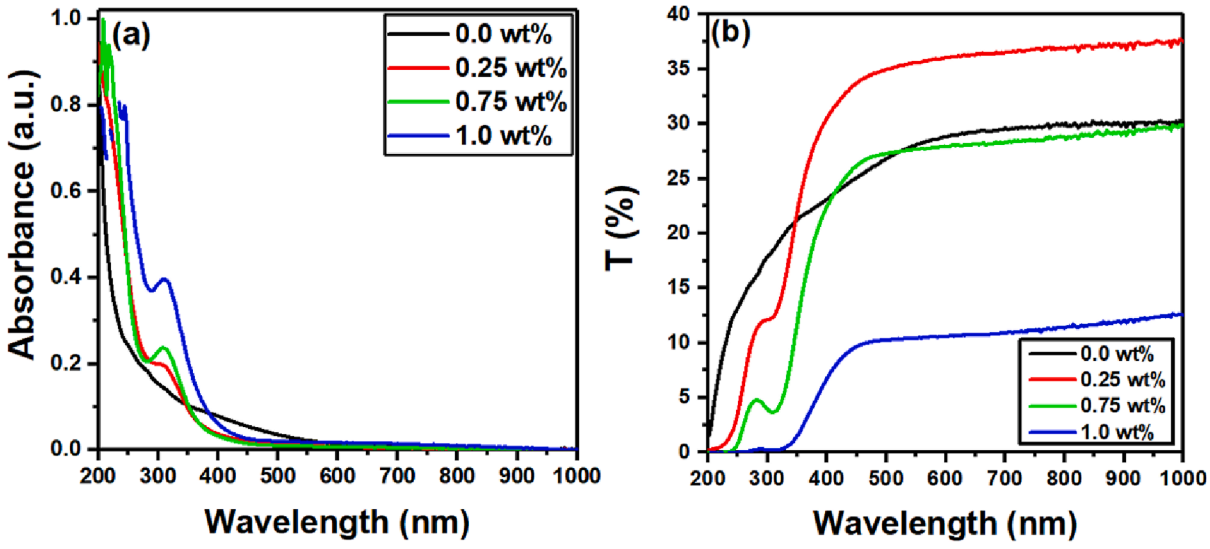

Fig. 4. Variation of (a) absorbance vs. wavelength, and (b) optical transmittance vs. wavelength for the PVDF nanocomposites consisting of 0.0, 0.25, 0.75, and 1 wt % of MoO_3/g-C_3N_4.

of optical dielectric loss function (ε_2) vs photon energy (hv). The dielectric loss function is calculated using the relation ($\varepsilon_{2=}$ 2nK) [38]. In the plot of (ε_2) vs (hv) the values of the energy gap are obtained by plotting the linear component to the intercept with the (hv). Energies of direct band gap are listed in Table 2 and the intercept value's expression of the real energy gap are in agreement with direct band gap illustrated from the plot in Fig. 5(b) and Table 1.

The relation below defines the strength of single oscillator (*f*) [39,40];

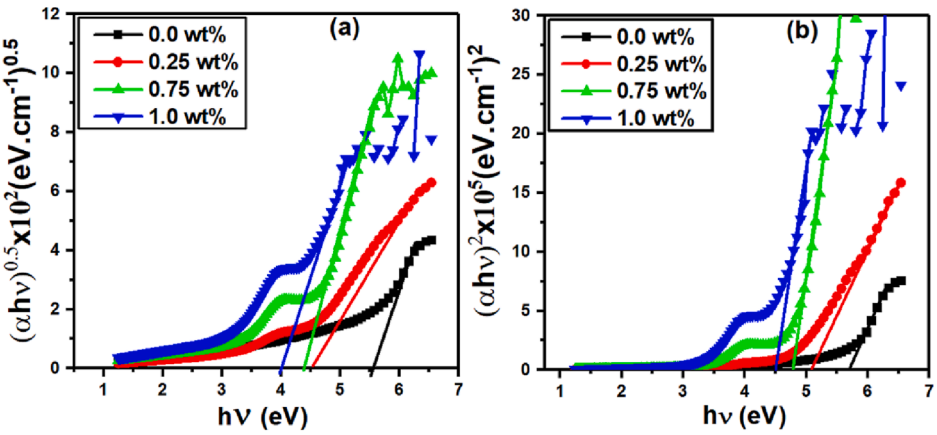

Fig. 5. Graphs of (a) $(\alpha h \upsilon)^{1/2}$ vs. h υ, and (b) $(\alpha h \upsilon)^{2}$ vs. h υ for the for the PVDF-MoO_3/g-C_3N_4 nanocomposites.

Table 1
Optical parameters of MoO_3/g-C_3N_4 nanocomposites.

MoO_3/g-C_3N_4 wt%	E_{dir}	E_{ind}	E_0	E_d	n_0	f (eV^2)
0.0	5.71	5.56	6.79	71.89	3.14	487.80
0.25	5.10	4.50	4.31	19.65	2.36	84.67
0.75	4.78	4.40	3.98	20.44	2.48	81.30
1.0	4.50	4.0	3.79	52.91	3.87	200.80

$$f = E_d E_0 \tag{5}$$

The integration of MoO_3/g-C_3N_4 reduces the oscillator strength as shown in Table 1. The nonlinear optical analysis for the PVDF-MoO_3/g-C_3N_4 nanocomposites were completed for the linear optical susceptibility ($\chi^{(1)}$) and the third order nonlinear optical susceptibility ($x^{(3)}$). These parameters are presented by the following formula [41];

$$\chi^{(1)} = \frac{E_d/E_0}{4\pi}, x^{(3)} = 6.82 \times 10^{-15}(E_d/E_0)^4 \tag{6}$$

The calculated data of $x^{(1)}$ and $x^{(3)}$ presented in Table 2 reveal the improvement as the content of MoO_3/g-C_3N_4 increases. These data is comparable with that estimated for PVC, PVA and PMMA nanocomposites in the literature [42–44].

Another important parameter is the nonlinear refractive index (n_2), which is computed concerning $x^{(3)}$ and n_0 data [45];

$$n_2 = \frac{12\pi x^{(3)}}{n_0} \tag{7}$$

Table 2 contains the estimated values of n_2, which showed enhancement with the integration of MoO_3/g-C_3N_4. Further, the data of n_2 produced in the present investigation is higher than that obtained in the literature [46,47].

Fig. 8 shows the fluorescence spectra of PVDF/MoO_3/g-C_3N_4 polymer films. The pure PVDF film exhibits certain special UV emissive properties, with a peak fluorescence at 371 nm. The sharpness of this band improved as the concentration of MoO_3/g-C_3N_4 increased. The spectra of PVDF/MoO_3/g-C_3N_4 films showed an emission band at 437 nm that correspond to g-C_3N_4 [48–50]. The intensity of this band enhanced slightly as the content of MoO_3/g-C_3N_4 raised up to 1.0 wt%. The deconvolution of the PL spectra indicated that the positions of the fluorescence peaks is nearly the same because of the small amount of nanofiller (upto 1.0 wt%).

According to the crystal field model, the transitions at 459, 486 and 529 nm are likely caused by the Mo^{5+} d-d band transition of a severely deformed polyhedron (Mo-O) in an octahedral crystal field [51]. The deep level Mo^{5+} d^2_{yz}-d^2_{xz} transition is responsible for the band in the emission spectra at 457 nm and 486 nm [52]. Meanwhile, the intensity of these emission peaks slightly improved after increasing the content of MoO_3/g-C_3N_4. Therefore, the nanocomposites of PVDF-MoO_3/g-C_3N_4

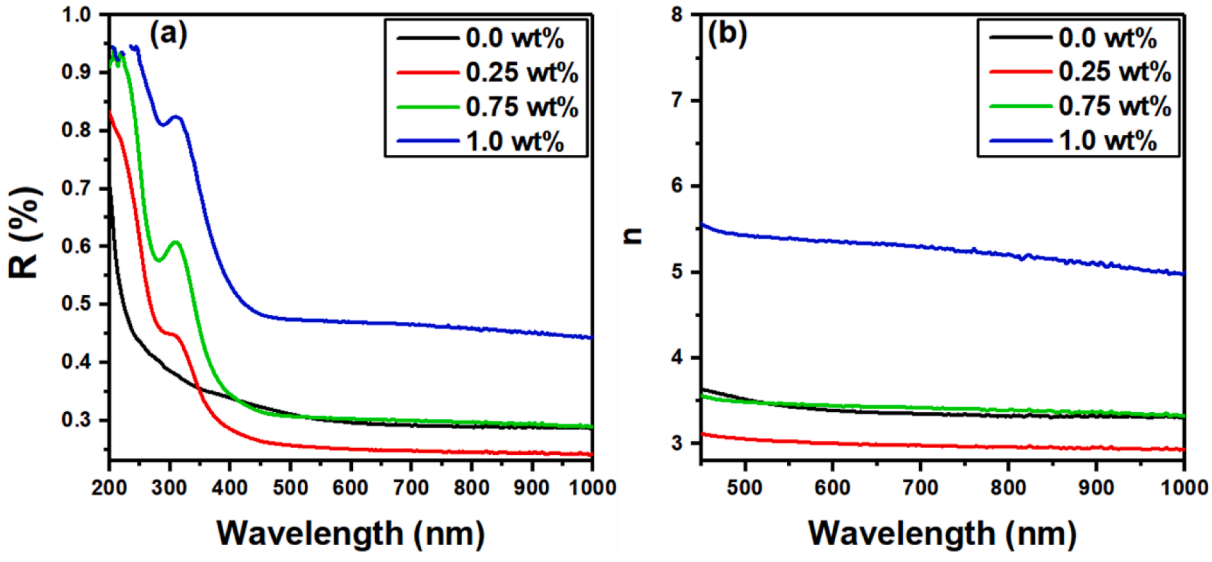

Fig. 6. Plots of (a) reflectance vs. wavelength, and (b) refractive index vs. wavelength, for the PVDF-MoO_3/g-C_3N_4 nanocomposites.

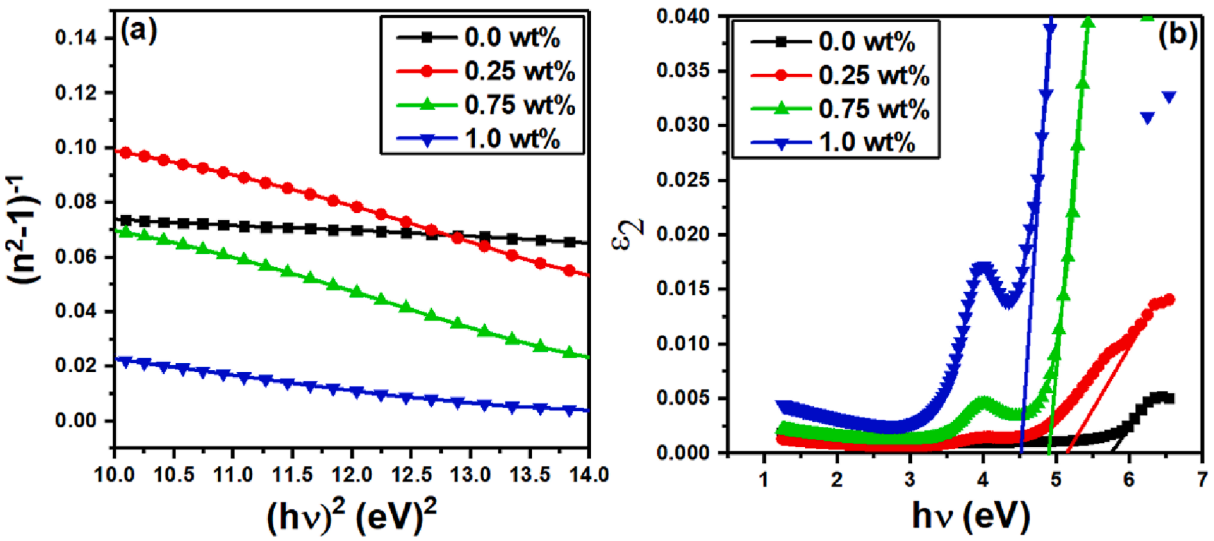

Fig. 7. Plots of (a) $(n^2\text{-}1)^{-1}$ vs. $h\upsilon^2$, and (b) ε_2 vs. h υ for the PVDF-MoO_3/g-C_3N_4 nanocomposites.

Table 2
Experiment data of optical susceptibility, nonlinear refreactive index and energy gap (E_{opt}) obtained from (ε_2) vs (hν) for the PVDF-MoO3/g-C3N4 nanocomposites.

MoO_3/g-C_3N_4 wt%	$\chi^{(1)}$ (esu)	$\chi^{(3)}$ (esu)	n_2 (esu)	E_{opt}
0.0	0.84	8.5×10^{-11}	9.5×10^{-10}	5.73
0.25	0.36	2.94×10^{-12}	4.7×10^{-11}	5.15
0.75	0.40	4.74×10^{-12}	7.22×10^{-11}	4.90
1.00	1.10	2.5×10^{-10}	2.5×10^{-9}	4.52

achieve precedence in optoelectronic applications because of distinctive optical characteristics.

Conclusions

This study investigates the structural and optical properties for prepared polymer nanocomposites of PVDF at different content of MoO_3/g-C_3N_4. The XRD diffraction patterns of PVDF with different concentrations of MoO_3/g-C_3N_4 have two characteristic peaks at 2 θ = 18.4° which was assigned to α-phase and 20.3° assigned to β-phase. The ESEM micrographs of PVDF-MoO_3/g-C_3N_4 nanocomposites have shown smooth surface topography. According to the UV–visible absorption spectra, the UV absorption of PVDF was increased when adding MoO_3/g-C_3N_4 nanoparticles where distinct peak was appeared in the UV region at 310 nm and its edges become more intense and moved towards higher wavelength after MoO_3/g-C_3N_4 incorporation. The optical values of (E_{dir}) and (E_{ind}) energies have decreased with increasing the nanoparticle composites content. The optical band gap energy (E_{opt}) was decreasing from 5.71 eV to 4.50 eV as increasing the content of MoO_3/g-C_3N_4. The refractive index (n) was increased with increasing the concentration of MoO_3/g-C_3N_4 in nanocomposites samples, except for the sample with 0.25 wt%. The distinctive optical characteristics of PVDF-MoO_3/g-C_3N_4 qualify such polymer nanocomposites for optoelectronic applications.

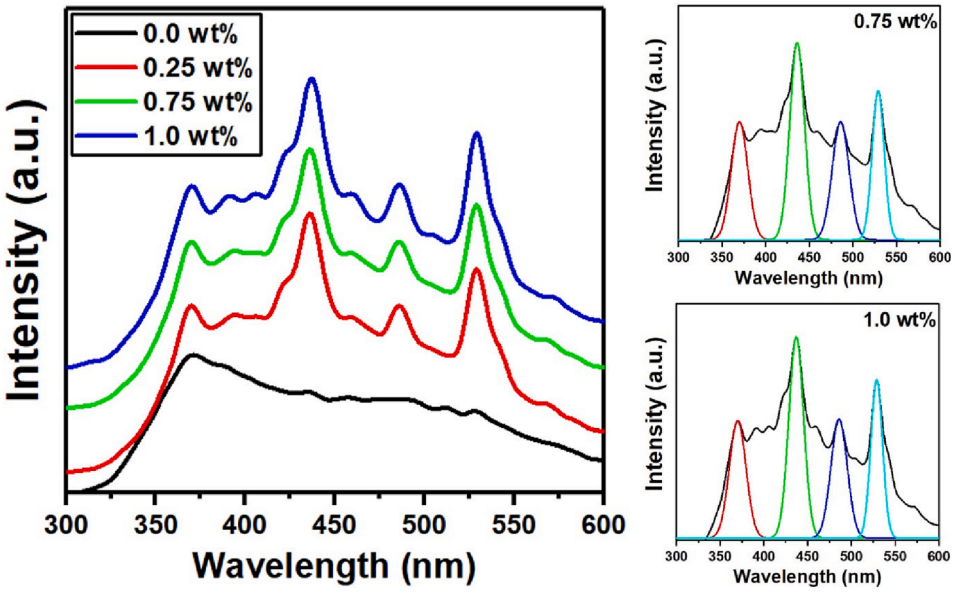

Fig. 8. Plots of PL intensity vs wavelength for the PVDF-MoO_3/g-C_3N_4 nanocomposites.

Funding

The authors extend their appreciation to the Deputyship for Research & Innovation, Ministry of Education in Saudi Arabia for funding this research work through the project number 223202.

Declaration of Competing Interest

The authors declare that they have no known competing financial interests or personal relationships that could have appeared to influence the work reported in this paper.

Data availability

No data was used for the research described in the article.

Acknowledgment

The authors gratefully acknowledge the central lab at Jouf University for providing the advance experiments methods used in this manuscript.

References

[1] Wu H, Fahy WP, Kim S, Kim H, Zhao N, Pilato L, et al. Recent developments in polymers/polymer nanocomposites for additive manufacturing. Prog Mater Sci 2020;111.
[2] Luo H, Zhou X, Ellingford C, Zhang Y, Chen S, Zhou K, et al. Interface design for high energy density polymer nanocomposites. Chem Soc Rev 2019;48(16):4424–65.
[3] Loste J, Lopez-Cuesta JM, Billon L, Garay H, Save M. Transparent polymer nanocomposites: An overview on their synthesis and advanced properties. Prog Polym Sci 2019;89:133–58.
[4] Sun X, Huang C, Wang L, Liang L, Cheng Y, Fei W, Li Y. Recent progress in graphene/polymer nanocomposites. Adv Mater 2021;33(6):2001105.
[5] Prateek, Bhunia R, Siddiqui S, Garg A, Gupta RK. Significantly enhanced energy density by tailoring the interface in hierarchically structured TiO2–BaTiO3–TiO2 nanofillers in PVDF-based thin-film polymer nanocomposites. ACS Appl Mater Interfaces 2019;11(15):14329–39.
[6] Singh D, Singh N, Garg A, Gupta RK. Engineered thiol anchored Au-BaTiO3/PVDF polymer nanocomposite as efficient dielectric for electronic applications. Compos Sci Technol 2019;174:158–68.
[7] Taha TA, Mahmoud MH, Hamdeh HH. Development, thermal and dielectric investigations of PVDF-Y2O3 polymer nanocomposite films. J Polym Res 2021;28(5):1–9.
[8] Dhatarwal P, Sengwa RJ. Tunable β-phase crystals, degree of crystallinity, and dielectric properties of three-phase PVDF/PEO/SiO2 hybrid polymer nanocomposites. Mater Res Bull 2020;129.
[9] Taha TA, El-Nasser KS. Synthesis, thermal and dielectric investigations of PVDF/PVP/Co0. 6Zn0. 4Fe2O4 polymer nanocomposite films. J Mater Sci Mater Electron 2021;32(23):27339–47.
[10] Patel PK, Rani J, Yadav KL. Effective strategies for reduced dielectric loss in ceramic/polymer nanocomposite film. Ceram Int 2021;47(7):10096–103.
[11] Hu J, Liu Y, Zhang S, Tang B. Novel designed core–shell nanofibers constituted by single element-doped BaTiO3 for high-energy–density polymer nanocomposites. Chem Eng J 2022;428.
[12] Indolia AP, Gaur MS. Optical properties of solution grown PVDF-ZnO nanocomposite thin films. J Polym Res 2013;20(1):1–8.
[13] Panda M, Sultana N, Singh AK. Structural and optical properties of PVDF/GO nanocomposites. Fullerenes, Nanotubes, Carbon Nanostruct 2022;30(5):559–70.
[14] El-Metwally EG, Nasrallah DA, Fadel M. The effect of Li4Ti5O12 nanoparticles on structural, linear and third order nonlinear optical properties of PVDF films. Mater Res Express 2019;6(8).
[15] El-Masry MM, Ramadan R. The effect of CoFe2O4, CuFe2O4 and Cu/CoFe2O4 nanoparticles on the optical properties and piezoelectric response of the PVDF polymer. Appl Phys A 2022;128(2):1–13.
[16] Gaur AM, Rana DS. Structural, optical and electrical properties of MgCl2 doped polyvinylidene fluoride (PVDF) composites. J Mater Sci Mater Electron 2015;26(2):1246–51.
[17] Ragg R, Natalio F, Tahir MN, Janssen H, Kashyap A, Strand D, et al. Molybdenum trioxide nanoparticles with intrinsic sulfite oxidase activity. ACS Nano 2014;8(5):5182–9.
[18] Navas I, Vinodkumar R, Mahadevan Pillai VP. Self-assembly and photoluminescence of molybdenum oxide nanoparticles. Appl Phys A 2011;103(2):373–80.
[19] Gwinner MC, Pietro RD, Vaynzof Y, Greenberg KJ, Ho PK, Friend RH, Sirringhaus H. Doping of organic semiconductors using molybdenum trioxide: a quantitative time-dependent electrical and spectroscopic study. Adv Funct Mater 2011;21(8):1432–41.
[20] Giannakopoulou T, Papailias I, Todorova N, Boukos N, Liu Y, Yu J, Trapalis C. Tailoring the energy band gap and edges' potentials of g-C3N4/TiO2 composite photocatalysts for NOx removal. Chem Eng J 2017;310:571–80.
[21] Zhu D, Zhou Q. Nitrogen doped g-C3N4 with the extremely narrow band gap for excellent photocatalytic activities under visible light. Appl Catal B 2021;281.
[22] Hayat A, Sohail M, Iqbal W, Taha TA, Alenad AM, Al-Sehemi AG, et al. Molecular engineering optimized carbon nitride photocatalyst for CO2 reduction to solar fuels. J Sci: Adv Mater Devices 2022;7(4).
[23] Chen Y, Lu C, Xu L, Ma Y, Hou W, Zhu JJ. Single-crystalline orthorhombic molybdenum oxide nanobelts: synthesis and photocatalytic properties. CrstEngComm 2010;12(11):3740–7.
[24] Taha TA, Mahmoud MH. Synthesis and characterization of PVDF-Er2O3 polymer nanocomposites for energy storage applications. Mater Chem Phys 2021;270.
[25] Alshammari AH, Alshammari M, Alshammari K, Allam NK, Taha TA. PVC/PVP/SrTiO3 polymer blend nanocomposites as potential materials for optoelectronic applications. Results Phys 2022;106173.
[26] Vidhate S, Shaito A, Chung J, D'Souza NA. Crystallization, mechanical, and rheological behavior of polyvinylidene fluoride/carbon nanofiber composites. J Appl Polym Sci 2009;112(1):254–60.
[27] Song R, Yang D, He L. Effect of surface modification of nanosilica on crystallization, thermal and mechanical properties of poly (vinylidene fluoride). J Mater Sci 2007;42(20):8408–17.
[28] Khalifa M, Mahendran A, Anandhan S. Synergism of graphitic-carbon nitride and electrospinning on the physico-chemical characteristics and piezoelectric properties of flexible poly (vinylidene fluoride) based nanogenerator. J Polym Res 2019;26(3):1–13.
[29] Liu R, Li X, Huang J, Pang H, Wan Q, Luo K, et al. Synthesis and Characterization of g-C3N4/Ag3PO4/TiO2/PVDF Membrane with Remarkable Self-Cleaning Properties for Rhodamine B Removal. Int J Environ Res Public Health 2022;19(23):15551.
[30] Indolia Ajay Pal, Gaur MS. Optical properties of solution grown PVDF-ZnO nanocomposite thin films. J Polym Res 2013;20(1):1–8.
[31] Sangiorgi N, Aversa L, Tatti R, Verucchi R, Sanson A. Spectrophotometric method for optical band gap and electronic transitions determination of semiconductor materials. Opt Mater 2017;64:18–25.
[32] Dolgonos A, Mason TO, Poeppelmeier KR. Direct optical band gap measurement in polycrystalline semiconductors: a critical look at the Tauc method. J Solid State Chem 2016;240:43–8.
[33] Kravets VG, Marshall OP, Nair RR, Thackray B, Zhukov A, Leng J, Grigorenko AN. Engineering optical properties of a graphene oxide metamaterial assembled in microfluidic channels. Opt Express 2015;23(2):1265–75.
[34] Bhunia R, Das S, Hussain S, Sehgal G, Chakraborty BR, Bhar R, Pal AK. Structural and optical properties of manganese-doped NanocrystallineZinc oxide/polyvinylidene fluoride flexible composite thin films deposited by the sol-gel method. Adv Polym Tech 2018;37(1):60–70.
[35] El-naggar AM, Heiba ZK, Mohamed MB, Kamal AM, Osman MM, Albassam AA, et al. Improvement of the optical characteristics of PVA/PVP blend with different concentrations of SnS2/Fe. J Vinyl Add Tech 2022;28(1):82–93.
[36] Tanaka K, Adachi S, Chujo Y. Side-chain effect of octa-substituted POSS fillers on refraction in polymer composites. J Polym Sci A Polym Chem 2010;48(24):5712–7.
[37] Sakr GB, Yahia IS, Fadel M, Fouad SS, Romčević N. Optical spectroscopy, optical conductivity, dielectric properties and new methods for determining the gap states of CuSe thin films. J Alloy Compd 2010;507(2):557–62.
[38] Kurt A. Influence of AlCl_3 on the optical properties of new synthesized 3-armed poly (methyl methacrylate) films. Turk J Chem 2010;34(1):67–80.
[39] Gündüz B. Optical properties of poly [2-methoxy-5-(3′, 7′-dimethyloctyloxy)-1, 4-phenylenevinylene] light-emitting polymer solutions: effects of molarities and solvents. Polym Bull 2015;72(12):3241–67.
[40] Banerjee M, Jain A, Mukherjee GS. Microstructural and optical properties of polyvinyl alcohol/manganese chloride composite film. Polym Compos 2019;40(S1):E765–75.
[41] Hassanien AS, Sharma I. Optical properties of quaternary a-Ge15-x Sbx Se50 Te35 thermally evaporated thin-films: refractive index dispersion and single oscillator parameters. Optik 2020;200.
[42] Taha TA, Hendawy N, El-Rabaie S, Esmat A, El-Mansy MK. Effect of NiO NPs doping on the structure and optical properties of PVC polymer films. Polym Bull 2019;76(9):4769–84.
[43] Soliman TS, Vshivkov SA, Elkalashy SI. Structural, linear and nonlinear optical properties of Ni nanoparticles–Polyvinyl alcohol nanocomposite films for optoelectronic applications. Opt Mater 2020;107.
[44] Kulyk B, Sahraoui B, Krupka O, Kapustianyk V, Rudyk V, Berdowska E, et al. Linear and nonlinear optical properties of ZnO/PMMA nanocomposite films. J Appl Phys 2009;106(9).
[45] AlAbdulaal TH, Yahia IS. Analysis of optical linearity and nonlinearity of Fe3+-doped PMMA/FTO polymeric films: new trend for optoelectronic polymeric devices. Phys B Condens Matter 2021;601.
[46] Tripathi SK, Kaur R. Investigation of non-linear optical properties of CdS/PS polymer nanocomposite synthesized by chemical route. Opt Commun 2015;352:55–62.
[47] Abdelhamied MM, Atta A, Abdelreheem AM, Farag ATM, El Sherbiny MA. Oxygen ion induced variations in the structural and Linear/Nonlinear optical properties of the PVA/PANI/Ag nanocomposite film. Inorg Chem Commun 2021;133.
[48] Yousefi R, Azimi HR, Mahmoudian MR, Basirun WJ. The effect of defect emissions on enhancement photocatalytic performance of ZnSe QDs and ZnSe/rGO nanocomposites. Appl Surf Sci 2018;435:886–93.

[49] Saray AM, Zare-Dehnavi N, Jamali-Sheini F, Yousefi R. Type-II p (SnSe)-n (g-C3N4) heterostructure as a fast visible-light photocatalytic material: Boosted by an efficient interfacial charge transfer of pn heterojunction. J Alloy Compd 2020;829.
[50] Tabar MB, Azimi H, Yousefi R. The Se role as a mediator to enhance the photocatalytic performance of the ZnSe/g-C3N4 nanocomposites. Appl Surf Sci 2023;156912.
[51] Sharma RK, Reddy GB. Synthesis and characterization of α-MoO3 microspheres packed with nanoflakes. J Phys D Appl Phys 2014;47(6).
[52] Sharma RK, Reddy GB. Effect of substrate temperature on the characteristics of α-MoO3 hierarchical 3D microspheres prepared by facile PVD process. J Alloy Compd 2014;598:177–83.